Effects of Imperfections on Solid-Wave Gyroscope Dynamics

Erdal Yilmaz, *Member, IEEE,* and David Bindel, *Member, IEEE*

***Abstract*—Solid-wave gyroscopes are symmetric resonators that sense rotation by measuring how Coriolis forces perturb a degenerate mode pair. The idealized dynamics of these devices are described by ODE models of two identical oscillators coupled by a perturbation due to rotation. In miniaturized solid-wave gyroscopes, geometric distortions due to imperfect fabrication also perturb the dynamics, and this limits sensing accuracy. In this work, we describe how geometric imperfections affect the dynamics of solid-wave gyroscopes. We also use selection rules both to find qualitative information about what types of geometry perturbations most affect sensor performance and to accelerate computations.**

I. Introduction

When a vibrating structure is placed in a rotating frame, non-inertial forces affect how the structure vibrates. For small and slowly-varying rates of rotation, the Coriolis force is the dominant non-inertial force. The Coriolis force brings a handedness to the system, since it involves cross products with the direction of rotation. For axisymmetric structures, the rotation breaks the symmetry of the dynamics: similar to the Doppler effect, elastic waves appear to travel faster or slower depending on the direction in which they travel relative to the rotation. Because of this symmetry breaking, the Coriolis force perturbs degenerate vibration modes in a way that splits their frequencies in proportion to the rate of rotation. The superposition of beating elastic waves forms a vibration pattern that rotates in the non-inertial frame in the direction opposite the frame rotation. The angle that the vibration pattern rotates is proportional to the total rotation experienced by the frame. The proportionality constant is called *Bryan's factor* (BF) in honor of G. H. Bryan, who in an 1890 experiment observed and explained the beating sound produced by a ringing wine glass placed on a rotating table [3]. When such an axisymmetric structure is used as a gyroscope, the beat frequency provides a good measure of the rate of rotation, and the rotation of the vibration pattern measures the total rotation of the frame. As a result there is no need for an external integrator for angle measurement. Axisymmetry also provides insensitivity of measurements to the rotation components in orthogonal directions. These properties made solid-wave gyrocopes popular for control applications that require high precision.

Today, hemispherical resonator gyroscopes are available commercially from Northrop Grumman, and have become the gyroscope of choice for satellites and other spacecraft [14]. The fabrication process used to make these gyroscopes produces highly axisymmetric structures, and includes steps that compensate for imperfections. Fabricating perfectly axisymmetric devices is impossible. Thus, post-processing steps and runtime methods that compensate for imperfections are common in practice.

In contrast to the expensive HRG fabrication process, MEMS fabrication techniques allow batch production of inexpensive sensors. The community has investigated ring resonators as rate-integrating gyroscopes for over a decade [1, 8], and has recently demonstrated several methods to fabricate hemispherical shells [4, 17, 19]. The key drawback to this approach is that microfabrication introduces geometric imperfections in many processing steps. These imperfections decrease the sensing accuracy considerably compared to macro gyroscopes. Understanding the nature of these imperfections is important for predicting sensor quality and formulating rules of thumb for device design.

In this paper, we describe the effect of fabrication imperfections on the dynamics of solid-wave gyroscopes. In the next section, we provide background on vibration analysis of axisymmetric structures and highlight prior work on gyro dynamics with imperfections. We also introduce a lumped model that plays a central role in our discussions. We describe the mapping of imperfections in the continuous domain to the perturbation coefficients in the lumped model. In the third section, we show how to describe imperfections in terms of a Fourier expansion; we also discuss types of imperfections in MEMS and provide a qualitative analysis of the corresponding Fourier series. In the fourth section, we give a description of selection rules and how they can be used to identify interactions between the vibration modes and perturbations. We also discuss the types of frequency splittings.

II. Background

In an axisymmetric structure, each mode shape has the form $u(r,z,\theta) = u^c(r,z)\cos(m\theta) + u^s(r,z)\sin(m\theta)$, where m is the *azimuthal number*. For each $m \geq 1$, if $u(r,z,\theta)$ is a mode shape, then $u(r,z,\theta+\pi/(2m))$ is a linearly independent mode shape with the same frequency; that is, the modes are *degenerate*. Since solid-wave gyros sense rotation through the splitting of degenerate mode frequencies, our main goal is to understand the dynamics of perturbed degenerate modes.

In a rotating frame, we write acceleration as

$$\mathbf{a} = \ddot{\mathbf{u}} + 2S\dot{\mathbf{u}} + (S^2 + \dot{S})(\mathbf{u} + \mathbf{r}) \tag{1}$$

where $\mathbf{u}$ is the displacement field, $\mathbf{r}$ is the position vector, and S is the skew-symmetric matrix encoding the rotation vector:

$$S = \begin{bmatrix} 0 & -\Omega_z & \Omega_y \\ \Omega_z & 0 & -\Omega_x \\ -\Omega_y & \Omega_x & 0 \end{bmatrix}. \tag{2}$$

This work was supported by DARPA MRIG Program.

The terms $2S\dot{u}$, $S^2(\mathbf{u}+\mathbf{r})$, and $\dot{S}(\mathbf{u}+\mathbf{r})$ respectively give the Coriolis force, centrifugal force, and Euler force. For small and slowly varying rates of rotation compared to the frequency of vibration, we can ignore the centrifugal and Euler forces.

In general, vibrations can be written as a superposition of modes:

$$\mathbf{u}(\mathbf{r},t) = \sum q_i(t)\mathbf{u}_i(\mathbf{r}). \tag{3}$$

By *dynamics*, we mean the behavior of $q_i(t)$ under forcing. We will consider dynamics in a two-dimensional space defined by an initially degenerate pair of mode shapes $\mathbf{u}_1, \mathbf{u}_2$:

$$\mathbf{u}(r,t) = q_1(t)\mathbf{u}_1(\mathbf{r}) + q_2(t)\mathbf{u}_2(\mathbf{r}). \tag{4}$$

A. Free Vibrations and Gyroscopic Splitting

Assuming time harmonic motion and discretizing the elasticity equations using finite elements, we arrive at a quadratic eigenvalue problem for free vibrations in a rotating frame:

$$\left[-\omega^2\mathbf{M} + i\omega\mathbf{B} + \mathbf{K}\right] u = 0, \tag{5}$$

where u is a vector of nodal displacements. When there is no rotation, we have the generalized eigenvalue problem

$$\mathbf{K}\hat{u} = \hat{\omega}^2\mathbf{M}\hat{u}. \tag{6}$$

The solutions of (6) belong to *invariant subspaces*, each associated with a specific frequency and azimuthal number m. For $m = 0$, the breathing modes, these subspaces are one-dimensional; for $m \geq 1$, they are two-dimensional [12].

In general, the rate of rotation is much smaller than the rate of vibration of the device, and so we can treat the Coriolis term, $i\omega\mathbf{B}$, in the quadratic system (5) as a perturbation to the generalized eigensystem (6). The projection onto the two-dimensional *unperturbed* invariant subspace, $\mathbf{V} = \begin{bmatrix}\hat{\mathbf{u}}_1 & \hat{\mathbf{u}}_2\end{bmatrix}$, provides us with two equations to compute the frequency split. The projected system has the simple form

$$(-\omega^2\mu\mathbf{I} + i\omega\Omega b\mathbf{J} + k\mathbf{I})\tilde{q} = 0, \tag{7}$$

where Ω is the rotation component in the direction of the symmetry axis and

$$\mathbf{V}^T\mathbf{M}\mathbf{V} = \mu\mathbf{I} \tag{8}$$

$$\mathbf{V}^T\mathbf{K}\mathbf{V} = k\mathbf{I} \tag{9}$$

$$\mathbf{V}^T\mathbf{B}\mathbf{V} = \Omega b\mathbf{J} \tag{10}$$

where μ, b, and k are scalar coefficients, the vector $\tilde{q}$ represents the amplitudes of the coordinates $q = \begin{bmatrix}q_1 & q_2\end{bmatrix}^T$, and

$$\mathbf{I} = \begin{bmatrix}1 & 0\\ 0 & 1\end{bmatrix}, \qquad \mathbf{J} = \begin{bmatrix}0 & -1\\ 1 & 0\end{bmatrix}. \tag{11}$$

Using perturbation theory, one can show that the frequency split and Bryan's factor are given by equations [10]:

$$\Delta\omega = \Omega\frac{b}{2\mu} \qquad \text{BF} = \frac{\Delta\omega}{m\Omega} = \frac{b}{2m\mu} \tag{12}$$

This frequency splitting due to the Coriolis term is the mechanism by which we sense rotation. However there might be other factors that result in frequency splittings.

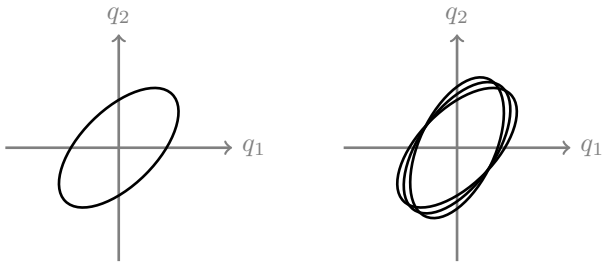

Fig. 1. Due to rotation, the elliptical trajectory rotates in the configure space.

B. Ideal Gyroscope Dynamics

We now consider the projected dynamical equations in the time domain. We will analyze the dynamics in $\mathbf{V}$,

$$\mathbf{u}(\mathbf{r},t) \approx \mathbf{V}(\mathbf{r})q(t). \tag{13}$$

Our goal is to understand how q_1 and q_2 evolve both in an ideal case and under various imperfections.

After normalizing the mass matrix, we write the second-order coupled equations for the ideal gyroscope as:

$$\ddot{q} + \gamma\Omega\mathbf{J}\dot{q} + \hat{\omega}^2\mathbf{I}q = 0 \tag{14}$$

The coupling due to the Coriolis force is captured by the geometry-dependent constant $\gamma = b/\mu$.

A full dynamical picture of a second-order system in two variables requires a four-dimensional phase space. However, we can visualize the motion using parametrized trajectories in the configuration space (q_1, q_2). Understanding the shape of the trajectory and its time evolution is important for sensor readout and for stabilizing the gyroscope [15].

When the system is not rotating, the trajectory in the configuration space is an ellipse. With appropriate initial conditions the ellipse becomes a straight line. A non-zero rotation causes the ellipse to rotate (Figure 1). The angle of rotation of the shape is proportional to the angle of rotation of the frame, and the constant of proportionality is BF. In the slow rotation approximation, it is possible to express the shape evolution by converting the lumped system into first-order ODEs for the orbital parameters of an elliptic motion [7].

C. Perturbed Gyroscope Dynamics

In order to account for perturbations, we can add phenomenological coefficients to the linear second-order model:

$$\ddot{q} + \mathbf{D}\dot{q} + \mathbf{C}q = 0 \tag{15}$$

where the matrices $\mathbf{C}$ and $\mathbf{D}$ include perturbations:

$$\tilde{\mathbf{D}} = \gamma\Omega\mathbf{J} - \mathbf{D} \tag{16}$$

$$\tilde{\mathbf{C}} = \hat{\omega}^2\mathbf{I} - \mathbf{C} \tag{17}$$

We interpret the off-diagonal elements of $\tilde{\mathbf{D}}$ and $\tilde{\mathbf{C}}$ as *anisodamping* and *anisoelasticity* respectively. Earlier, researchers investigated the dependence of trajectories on various coefficients of these perturbing matrices [7, 11, 16].

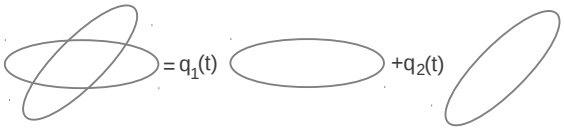

Fig. 2. A vibration at a pure frequency for $m \geq 1$ is a linear combination of modal shapes of the doublet. In the figure $m = 2$ modes are depicted. $\mathbf{u}(\mathbf{r}, t) = q_1(t)\mathbf{u}_1(\mathbf{r}) + q_2(t)\mathbf{u}_2(\mathbf{r})$

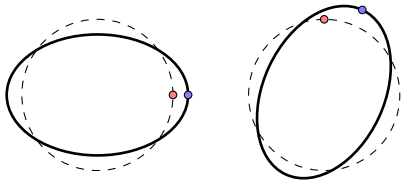

Fig. 3. In the non-rotating frame, the point on the vibrating pattern rotates less than the material point on the ring.

D. Geometric Perturbations

We consider the distorted geometry of the resonator and construct the system matrices for the discrete model (5):

$$\tilde{\mathbf{M}} = \mathbf{M} + \delta\mathbf{M} \tag{18}$$

$$\tilde{\mathbf{K}} = \mathbf{K} + \delta\mathbf{K} \tag{19}$$

$$\tilde{\mathbf{B}} = \mathbf{B} + \delta\mathbf{B} \tag{20}$$

Projecting onto the subspace $\mathbf{V}$, we recover perturbed lumped system governing the dynamics:

$$\mathbf{V}^T\tilde{\mathbf{M}}\mathbf{V} = \check{\mathbf{M}} \tag{21}$$

$$\mathbf{V}^T\tilde{\mathbf{K}}\mathbf{V} = \check{\mathbf{K}} \tag{22}$$

$$\mathbf{V}^T\tilde{\mathbf{B}}\mathbf{V} = \check{\mathbf{B}} \tag{23}$$

Mass orthogonalization in the perturbed system requires a change of basis for the subspace $\mathbf{V}$ in the form $\tilde{\mathbf{V}} = \mathbf{V}\mathbf{Y}$,

$$\mathbf{Y}^T\check{\mathbf{M}}\mathbf{Y} = \mathbf{I} \tag{24}$$

A natural choice for $\mathbf{Y}$ is $\mathbf{Y} = \check{\mathbf{M}}^{-1/2}$. Hence we can construct $\mathbf{D}$ and $\mathbf{C}$ using

$$\mathbf{D} = \check{\mathbf{M}}^{-\frac{1}{2}}\check{\mathbf{B}}\check{\mathbf{M}}^{-\frac{1}{2}} \tag{25}$$

$$\mathbf{C} = \check{\mathbf{M}}^{-\frac{1}{2}}\check{\mathbf{K}}\check{\mathbf{M}}^{-\frac{1}{2}} \tag{26}$$

from which we compute $\tilde{\mathbf{D}}$ and $\tilde{\mathbf{C}}$.

E. Ring Resonators

One of the simplest resonator geometries is a ring. At its center, the resonator is attached to a rotating body. As the body rotates, the vibration pattern rotates in opposite direction in a reference frame fixed on the body. Within this frame, measuring the angle rotated by the vibration pattern and dividing it by BF, we compute the total angle rotated by the body in space. (Figure 3).

Beam and shell models are the most common tools for analyzing thin rings. Bryan himself explained the results of his wineglass experiment by considering a ring resonator using a beam model [3]. Approximations provided by these models enabled investigations of the effects of imperfections. Researchers have analyzed frequency splittings and vibration localization in deformed ring resonators [2], and they also demonstrated trimming of frequencies using point masses [13]. In addition to geometric imperfections, it is also possible to study the frequency splittings resulting from the anisotropy of resonator material [5].

III. Imperfections

We consider perturbations of an ideal axisymmetric geometry by a mapping in cylindrical coordinates $(\tilde{r}, \tilde{z}, \tilde{\theta}) = (r, z, \theta) + \epsilon f(r, z, \theta)$. The function f represents a perturbation shape, and ϵ is the amplitude of perturbation. In general, we write f as a Fourier series in θ:

$$f(r, z, \theta) = \sum_p A_p(r, z)\cos(p\theta + \phi_p) \tag{27}$$

We pay special attention to the case $f = A(r, z)\cos(p\theta)$; in this case, we refer to p as the *perturbation mode*.

As an example, we consider an imperfect ring resonator with nominal radius R and thickness h (Figure 4). We compute eigenfrequencies in two-dimensions using the finite element method under plane-strain assumption. For convenience, we work on the unperturbed domain. Since the perturbations $\delta\mathbf{M}$, $\delta\mathbf{K}$, $\delta\mathbf{B}$ are functionals of imperfections, we express them as variations of integrals on the unperturbed domain via mappings between the perfect and imperfect annular regions.

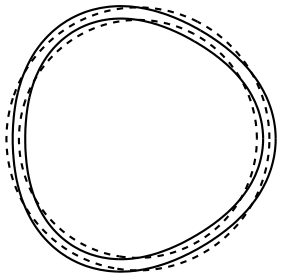

Fig. 4. Distorted ring geometry

A. Imperfections in MEMS Fabrication

Some MEMS fabrication errors can be characterized by a symmetry or a few dominant terms in the Fourier expansion of the geometry:

1) Isotropic under/over etch effects do not disturb the symmetry ($p = 0$ mode).
2) Thickness variation across a device due to proximity to a gas jet will generally be a linear function of x (distance from the gas inflow); this is a $p = 1$ mode perturbation to the geometry.
3) Similarly, variations in sidewall slant during a reactive ion etch are basically explained by variation in the angle to the ion source; this is again basically a $p = 1$ mode.
4) Mask misalignment effects are primarily $p = 1$ mode.
5) Any effects that might stretch things slightly along a single axis are $p = 2$.

6) "Squaring-off" effects due to anisotropy of etch in a 100 wafer are primarily in the $p = 4$ mode; more generally, these perturbations have the symmetry group of the square. Similarly, in a 111 wafer $p = 3$ mode is more relevant.

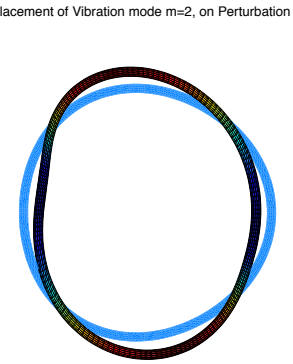

Fig. 5. Vibration of a perturbed geometry. The perturbation shape is $f(r, \theta) = \cos(3\theta)$; the superimposed mode shape is at $m = 2$.

IV. Selection Rules and Frequency Splittings

The symmetries of the device geometry and the perturbations lead us to use group theory together with perturbation theory in order to analyze frequency splittings. Similar tools have been in the toolset for atomic and molecular physicists [ey: citation]. We can easily draw conclusions whether the frequencies will split or not as a result of imperfections. We can also characterize the order of splittings. To validate our observations, the ring resonator provides an excellent example. Researchers have studied geometric imperfections of the ring resonator and quantified frequency splittings [6, 9].Beam and shell models employed restricts understanding to thin resonators with simple geometry. We use three-dimensional elasticity while exploiting axisymmetry. Our approach enables the study of more complex geometries in the same framework. Our observations from numerical studies produce the same results in that we see a first order splitting for modes $p = 2m$ and a second order splitting for modes $p = m$ as shown in Figures 7 and 8 respectively. For most of the values, the frequencies do not split, but decrease together. For example, $m = 2$ modes are not split by a perturbation mode $p = 3$ (Figure 5).

A. Selection Rules

We analyze whether a perturbation at azimuthal number p will split a particular degenerate vibration mode at azimuthal number m by considering the linear independence of the perturbed modal shapes. We expand the perturbed displacement field for a mode in a Fourier series: [•]

db deleted here

$$\mathbf{u}(r, z, \theta) = \sum_{j=-\infty}^{\infty} \mathbf{u}_j(r, z) \exp(ij\theta) \tag{28}$$

Since the perturbed geometry is p-fold rotationally symmetric, another modal displacement field at the same frequency is:

$$\hat{\mathbf{u}}(r, z, \theta) = \mathbf{u}(r, z, \theta + 2\pi/p) \tag{29}$$

$$\hat{\mathbf{u}}(r, z, \theta) = \sum_{j=-\infty}^{\infty} \mathbf{u}_j(r, z) \exp(ij\theta)\xi^j \tag{30}$$

$$= \sum_{j=-\infty}^{\infty} \hat{\mathbf{u}}_j(r, z) \exp(ij\theta) \tag{31}$$

where $\xi = \exp(i2\pi/p)$ and $\hat{\mathbf{u}}_j(r, z) = \mathbf{u}_j(r, z)\xi^j$. The fields are linearly dependent if $\mathbf{u} = \pm\hat{\mathbf{u}}$, which implies $\mathbf{u}_j = \pm\hat{\mathbf{u}}_j$ for all nonzero coefficients. The nonzero coefficients match only when $\xi^j = \pm 1$, which is only possible if $2\pi j/p = l\pi$ for some integer l. Unless p divides $2j$, where j is the index of some nonzero Fourier coefficient of the displacement field, the degeneracy will remain intact. [db: consider rewriting the last sentence]. As a result we conclude, if geometry retains p-fold symmetry, it will leave vibration modes with azimuthal number m, where $p \nmid 2m$, degenerate.[ey: We are assuming the mode spectrum is highly concentrated at m]

From a computational point of view, symmetry implies the sparsity of the finite element system matrices (Figure 6).We use shape functions that are products of polynomials in (r, z) and trigonometric functions in θ. For such shape functions, the FE matrices involve angular integrals of the form:

$$\int_0^{2\pi} \begin{Bmatrix} \cos m\theta \\ \sin m\theta \end{Bmatrix} \begin{Bmatrix} \cos n\theta \\ \sin n\theta \end{Bmatrix} \begin{Bmatrix} \cos p\theta \\ \sin p\theta \end{Bmatrix} d\theta \tag{32}$$

Here, n is the azimuthal number of the virtual displacement. These terms may be nonzero only when $m \pm n \pm p = 0$. Thus, for a given p, only some of the blocks (m, n) of the system matrices will be nonzero.

[db: Switched from symmetry arguments to perturbation arguments] A first order change to the modes at m requires the perturbation to hit the block (m, m). This is possible for $p = 2m$ and $p = 0$, which explains the observed behavior from simulations (Figure 7).

Apart from decoupling the modes, another advantage of using a Fourier basis is that we may exploit the block structure of the FE matrices to speed up computations.

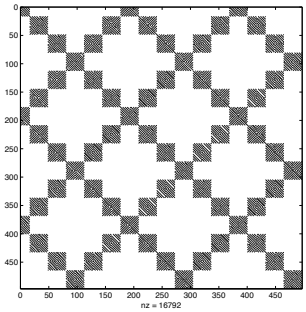

Fig. 6. Selection rules are used to compute only the relevant blocks of the system matrices. The figure shows the sparsity pattern for the stiffness matrix with $m \in [0 : 15], p = 6$.

B. Frequency Splittings

Based on the reasoning via selection rules, for many modes of the system, the degeneracy remains intact. However both frequencies experience a decrease as a quadratic function of the perturbation amplitude.

[ey: explain first and second order splittings]

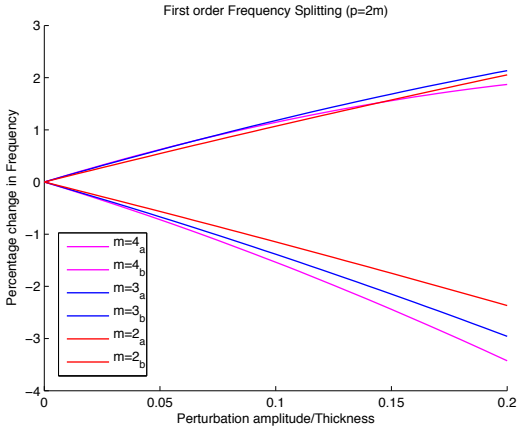

Fig. 7. First-order splittings of degenerate mode frequencies with azimuthal number m under a perturbation shape $f(r,\theta) = \cos(2m\theta)$.

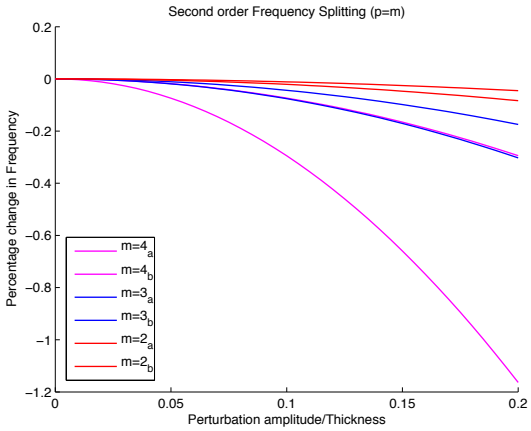

Fig. 8. Second-order splittings of degenerate mode frequencies with azimuthal number m under a perturbation shape $f(r,\theta) = \cos(m\theta)$.

For HRG, the working vibration mode is $m = 2$. However it has been observed that $m = 3$ mode is less sensitive to microfabrication imperfections.[ey: needs citations] If we take into account the mode number characterization of imperfections in the previous section, selection rules help us understand these observations. The $m = 2$ mode will be affected at first order by $p = 0$ (axisymmetric) and $p = 4$ (square symmetry) perturbations, but the only perturbation that we can guarantee will not effect degeneracy past first order is an axisymmetric perturbation. In contrast, the $m = 2$ mode will be affected at first order by $p = 0$ (axisymmetric) and $p = 6$ (hexagonal symmetry) perturbations, and perturbations that do not themselves have three-fold rotational symmetry ($p = 3l$) are guaranteed not to break degeneracy of the mode shapes. In particular, this means that, though the $m = 3$ shape

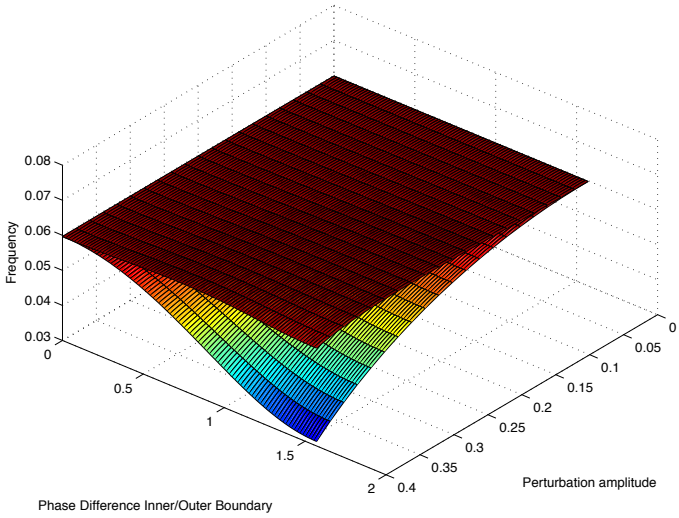

Fig. 9. Splitting of $m = 2$ mode on a ring with inner and outer boundaries perturbed by $f_{in}(r) = A\cos(2\theta)$ and $f_{out}(r) = A\cos(2\theta + \phi)$.

may be distorted, it will remain degenerate under most of the fabrication effects we consider.

Sorenson et al. observed the effects of thickness anisotropy. They fabricated a hemispherical resonator using wet thermal oxidation in which thickness depends on the crystal direction of the silicon surface it grows on. Comparing frequencies computed using FE for the lowest order modes at azimuthal numbers $m = 2$ and $m = 3$ of hemispherical shells fabricated using molds in (001) and (111) wafers, they argued parallel to our discussions [18].

V. Conclusion

Undesired effects of fabrication of solid-wave gyroscopes is a bottleneck in minituarization. Understanding the geometric imperfections due to fabrication processes and their effects on the working principles of these gyroscopes is critical for design and control. We summarized earlier explanations of phase space dynamics and provided a connection to compute relevant ODE coefficients using perturbation theory. Our approach to consider similarities with other symmetric physical systems and analysis with group theory lead into selection rules. We improved computational performance via block selection. We highlighted typical perturbation modes in MEMS fabrication of axisymmetric vibration structures and explained why $m = 3$ mode is less susceptible to geometric imperfections.

Acknowledgment

The authors would like to thank DARPA MRIG Program for supporting this project.

References

[1] F. Ayazi and K. Najafi. A harpss polysilicon vibrating ring gyroscope. *Microelectromechanical Systems, Journal of*, 10(2):169–179, 2001.

[2] Paolo Bisegna and Giovanni Caruso. Frequency split and vibration localization in imperfect rings. *Journal of Sound and Vibration*, 306(35):691 – 711, 2007.

[3] G. H. Bryan. On the beats in the vibrations of a revolving cylinder or bell. *Proceedings of the Cambridge Philosophical Society*, 7:101–111, 1890.

[4] J. Cho, J. Yan, J.A. Gregory, H. Eberhart, R.L. Peterson, and K. Najafi. High-q fused silica birdbath and hemispherical 3-d resonators made by blow torch molding. In *Micro Electro Mechanical Systems (MEMS), 2013 IEEE 26th International Conference on*, pages 177–180, 2013.

[5] R. Eley, C.H.J. Fox, and S. McWilliam. Anisotropy effects on the vibration of circular rings made from crystalline silicon. *Journal of Sound and Vibration*, 228(1):11 – 35, 1999.

[6] C.H.J. Fox, R.S. Hwang, and S. McWilliam. The in-plane vibration of thin rings with in-plane profile variations part ii: Application to nominally circular rings. *Journal of Sound and Vibration*, 220(3):517 – 539, 1999.

[7] B. Friedland and M. Hutton. Theory and error analysis of vibrating-member gyroscope. *Automatic Control, IEEE Transactions on*, 23(4):545–556, 1978.

[8] Guohong He and K. Najafi. A single-crystal silicon vibrating ring gyroscope. In *Micro Electro Mechanical Systems, 2002. The Fifteenth IEEE International Conference on*, pages 718–721, 2002.

[9] R.S. Hwang, C.H.J. Fox, and S. McWilliam. The in-plane vibration of thin rings with in-plane profile variations part i: General background and theoretical formulation. *Journal of Sound and Vibration*, 220(3):497 – 516, 1999.

[10] Stephan V. Joubert, Michael Y. Shatalov, and Temple H. Fay. Rotating structures and bryan's effect. *American Journal of Physics*, 77(6):520–525, 2009.

[11] Zhuravlev Victor P. Klimov, D. M. *Group-theoretic methods in mechanics and applied mathematics*. Taylor & Francis, New York, 2002.

[12] R. Perrin and T. Charnley. Group theory and the bell. *Journal of Sound and Vibration*, 31(4):411 – 418, 1973.

[13] A.K. Rourke, S. McWilliam, and C.H.J. Fox. Frequency trimming of a vibrating ring-based multi-axis rate sensor. *Journal of Sound and Vibration*, 280(35):495 – 530, 2005.

[14] David M. Rozelle. The hemispherical resonator gyro: From wineglass to the planets.

[15] A.M. Shkel, Roberto Horowitz, A.A. Seshia, Sungsu Park, and R.T. Howe. Dynamics and control of micromachined gyroscopes. In *American Control Conference, 1999. Proceedings of the 1999*, volume 3, pages 2119–2124 vol.3, 1999.

[16] M. Shkel, Roger T. Howe, , and Roberto Horowitz. Modeling and simulation of micromachined gyroscopes in the presence of imperfections. In *International Conference On Modeling and Simulation of Microsystems*, 1999.

[17] L.D. Sorenson, X. Gao, and F. Ayazi. 3-d micromachined hemispherical shell resonators with integrated capacitive transducers. In *Micro Electro Mechanical Systems (MEMS), 2012 IEEE 25th International Conference on*, pages 168–171, 2012.

[18] L.D. Sorenson, P. Shao, and F. Ayazi. Effect of thickness anisotropy on degenerate modes in oxide microhemispherical shell resonators. In *Micro Electro Mechanical Systems (MEMS), 2013 IEEE 26th International Conference on*, pages 169–172, 2013.

[19] K. Visvanathan, Tao Li, and Y.B. Gianchandani. 3d-soule: A fabrication process for large scale integration and micromachining of spherical structures. In *Micro Electro Mechanical Systems (MEMS), 2011 IEEE 24th International Conference on*, pages 45–48, 2011.

APPENDIX

The abstract for Sensors has several claims that are not obvious. These notes are meant to sketch out the reasoning in slightly more detail. The basic framework is that we are perturbing an ideal axisymmetric geometry by the mapping $(\tilde{r}, \tilde{z}, \tilde{\theta}) = (r, z, \theta) + \epsilon f(r, z, \theta)$, and we can reason about how frequencies change in terms of preserved symmetries and in terms of the symmetry of f.

A. Symmetry, selection rules, and perturbations

If operators A and B commute, they must have compatible eigenstructures – that is, maximal invariant subspaces of B are invariant for A, and vice-versa. This fact is helpful in deriving information about the eigenstructure of a problem based purely on generators for the symmetry group under which the perturbed problem remains invariant. Reasoning about how perturbations affect symmetry leads to *selection rules*, familiar in the study of quantum mechanics, for understanding how symmetry-breaking perturbations affect degeneracy.

Many perturbations of interest have a rotational symmetry $Gf = f$, where

$$Gw(r, z, \theta) = w(r, z, \theta + 2\pi/p)$$

is a generator for a representation of the group C_p. There are p maximal invariant subspaces for G, which gives the *canonical decomposition* of the space for the representation of the cyclic group:

$$\mathcal{U}_k = \left\{ \sum_{j=-\infty}^{\infty} c_j(r, z) \exp(i(k + jp)\theta) \right\}, \quad k = 0, 1, \ldots, p-1.$$

Except at $k = 0$ or $k = p/2$, these subspaces contain no (nonzero) purely real vectors; but for systems without damping, we can always choose a real system of eigenvectors. Thus, we have "physically irreducible" representations $\mathcal{V}_k = \mathcal{U}_k \oplus \mathcal{U}_{p-k}$ except for $k = 0$ and $k = p/2$; and modes in these spaces remain degenerate in the absence of damping. For $k = 0$ and $k = p/2$, we can write a real basis for $\mathcal{V}_k = \mathcal{U}_k$, so modes in these spaces are generally not degenerate.

Perturbations may also have the reflectional symmetry $Pf = f$, where

$$Pw(r, z, \theta) = w(r, z, -\theta).$$

The invariant subspaces for P are functions whose Fourier series consist of only sine terms ($Pw = -w$) and functions whose Fourier series consist only of cosine terms ($Pw = w$). In this case, the eigenvectors again must live in the same spaces $\mathcal{V}_k$ as above, with all modes degenerate for $k \notin \{0, p/2\}$.

We can say more if we combine symmetry with perturbation theory. Our problem in the idealized geometry involves an operator A_0 which is rendered block-diagonal in a Fourier basis, with no interactions between different azimuthal numbers, and a perturbation $\epsilon A_1 + O(\epsilon^2)$. If $f(r, z, \theta)$ has the form $f_c(r, z)\cos(p\theta) + f_s(r, z)\sin(p\theta)$, then the block (m, n) of A_1 involves integrals of purely sinusoidal functions at azimuthal numbers m, n, and p, and can only be nonzero if $m \pm n \pm p = 0$. Barring accidental degeneracies, the only way for the eigenvalues with wave number m in the ideal geometry can change at first order under the perturbation is if the perturbation is nonzero in the (m, m) block, i.e. if $p = 2m$ or $p = 0$. We reason about more complicated functions f by decomposing them across azimuthal numbers. In particular, a perturbation with p-fold rotational symmetry can only have nonzero Fourier coefficients at azimuthal numbers that are multiples of p; such a perturbation can only change the frequencies of modes with wave m at first order in the case that $2m = lp$. [ey: $(m, p, l) = (3, 2, 3)$ case?]

B. Application to MEMS gyroscopes

Some of the types of fabrication errors that occur in MEMS can be characterized by a symmetry or a few dominant terms in the Fourier expansion of the geometry:

1) Isotropic under/over etch effects do not disturb the symmetry ($p = 0$ mode).
2) Thickness variation across a device due to proximity to a gas jet will generally be a linear function of x (distance from the gas inflow); this is a $p = 1$ mode perturbation to the geometry.
3) Similarly, variations in sidewall slant during a reactive ion etch are basically explained by variation in the angle to the ion source; this is again basically a $p = 1$ mode.
4) Mask misalignment effects are primarily $p = 1$ mode.
5) Any effects that might stretch things slightly along a single axis are $p = 2$.
6) "Squaring-off" effects due to anisotropy of etch in a 111 wafer are primarily in the $p = 4$ mode; more generally, these perturbations have the symmetry group of the square.

The $m = 2$ mode will be affected at first order by $p = 0$ (axisymmetric) and $p = 4$ (square symmetry) perturbations, but the only perturbation that we can guarantee will not effect degeneracy past first order is an axisymmetric perturbation. In contrast, the $m = 2$ mode will be affected at first order by $p = 0$ (axisymmetric) and $p = 6$ (hexagonal symmetry) perturbations, and perturbations that do not themselves have three-fold rotational symmetry ($p = 3l$) are guaranteed not to break degeneracy of the mode shapes. In particular, this means that, though the $m = 3$ shape may be distorted, it will remain degenerate under most of the fabrication effects we consider.

NOMENCLATURE

$\mathbf{a}$	Acceleration in the rotating frame
$\mathbf{B}$	Gyroscopic matrix
$\mathbf{C}$	2×2 stiffness matrix
$\mathbf{D}$	2×2 damping matrix
$\mathbf{K}$	Stiffness matrix
$\mathbf{M}$	Mass matrix
$\mathbf{r}$	Position vector
$\mathbf{u}$	Displacement field
$\hat{\omega}$	Unperturbed angular frequency
$\hat{u}$	Unperturbed nodal displacement values
Ω	Rate of rotation of the frame
ω	Angular frequency
$\tilde{\mathbf{C}}$	Anisoelasticity matrix
$\tilde{\mathbf{D}}$	Anisodamping matrix
m	Azimuthal number of vibration mode
n	Azimuthal number for virtual displacement
S	Skew-symmetric matrix for $\Omega\times$
u	Vector of nodal displacements